


Crystal structure of palbociclib form A, C<sub>24</sub>H<sub>29</sub>N<sub>7</sub>O<sub>2</sub>

Petr Buikin,<sup>1,2</sup> Alexander Korlyukov,<sup>1</sup> Ivan Ushakov,<sup>1,†</sup> Alexander Goloveshkin,<sup>1</sup> Elizaveta Kulikova,<sup>3</sup> and Anna Vologzhanina <sup>1,a)</sup>

<sup>1</sup>A. N. Nesmeyanov Institute of Organoelement Compounds RAS, Vavilova str. 28, Moscow 119334, Russia

<sup>2</sup>Institute of General and Inorganic Chemistry RAS, Leninsky Prosp. 31, Moscow 119991, Russia

<sup>3</sup>Kurchatov Institute, National Research Center, Pl. Akad. Kurchatova 1, Moscow 123182, Russia

(Received 26 June 2024; accepted 19 August 2024)

The crystal structure of palbociclib (C<sub>24</sub>H<sub>29</sub>N<sub>7</sub>O<sub>2</sub>) used as a medication for the treatment of breast cancer has been solved and refined using synchrotron radiation after density functional theory optimization. Palbociclib crystallizes in the monoclinic system (space group *P*2<sub>1</sub>/*c*, #14) at room temperature with crystal parameters: *a* = 11.3133(2), *b* = 5.62626(9), *c* = 35.9299(9) Å, β = 101.5071(12), *V* = 2241.03(8) Å<sup>3</sup>, and *Z* = 4. The crystal structure contains infinite N–H⋯N bonded layers. The powder pattern has been submitted to ICDD for inclusion in the Powder Diffraction File™ (PDF®).

© The Author(s), 2024. Published by Cambridge University Press on behalf of International Centre for Diffraction Data.

[doi:10.1017/S0885715624000411]

Keywords: palbociclib, powder diffraction, Rietveld refinement

## I. INTRODUCTION

Palbociclib (DrugBank No DB09073) is a piperazine pyridopyrimidine used to treat HER2-negative and HR-positive advanced or metastatic breast cancer (Ibrahim et al., 2016). It is a second-generation cyclin-dependent inhibitor of the CDK4 and CDK6 kinases (Finn et al., 2009; Rocca et al., 2014). The systematic name is 6-acetyl-8-cyclopentyl-5-methyl-2-[[5-(piperazin-1-yl)pyridin-2-yl]amino]-7H,8H-pyrido[2,3-d]pyrimidin-7-one (C<sub>24</sub>H<sub>29</sub>N<sub>7</sub>O<sub>2</sub>). Figure 1 shows a two-dimensional molecular diagram of palbociclib.

Crystal structures of several palbociclib salts and a cocrystal are reported (Katiyar et al., 2021; Zhou et al., 2023; Allu et al., 2024). Patents US10329290B2 and US10766895B2 also contain information about the characteristic peaks in the X-ray powder diffraction patterns (PXRDs) for two crystal forms of palbociclib free base (Fan et al., 2019, 2020). However, the patterns have not been indexed, neither have the crystal structures of a free base palbociclib been solved and reported to date. Herein, we report on the crystal structure of form A of palbociclib as obtained using synchrotron radiation. This work is part of a project for determination of crystal structures of pharmaceutical ingredients from powder diffraction patterns (Goloveshkin et al., 2021, 2024; Buikin et al., 2024a, 2024b).

## II. EXPERIMENTAL

Palbociclib substance was purchased from Clearysynth (CAS No. 571190-30-2) and used without any purification. The synchrotron PXRD data were recorded at X-ray structural analysis beamline (Belok/XSA) of Kurchatov Synchrotron Radiation Source (Svetogorov et al., 2020). Monochromatic

radiation of wavelength 0.7500 Å was used to measure the pattern and then to determine the θ angles. The sample was placed in a cryoloop of 200 μm in size and rotated around the horizontal axis during the measurement, which made it possible to average the diffraction patterns according to the orientations of the sample. The diffraction pattern was collected by the 2D Rayonix SX165 detector, which was located at a distance of 250 mm with 18° tilt angle. Debye–Scherrer (transmission) geometry was used with a 400 μm beam size. The 2θ range was 0.32–38.125° with a step size of 0.005°. The total exposure time was 10 min. The two-dimensional powder diffraction pattern obtained on the detector was further integrated to the standard form of the dependence of the intensity on the scattering angle *I*(2θ) using Dionis software (Svetogorov, 2018). To calibrate the sample–detector distance, the polycrystalline LaB<sub>6</sub> (NIST SRM 660a, Morris et al., 1984) was used as a standard with the known positions of the diffraction lines. The diffraction peaks were approximated by fundamental parameters with Gaussian 1/cos(θ) convolution as described at ‘Bruker TOPAS 5 User Manual’ (2014).

The powder pattern was indexed in the P-centered monoclinic unit cell with the Topas 5.0 software (Coelho, 2003;

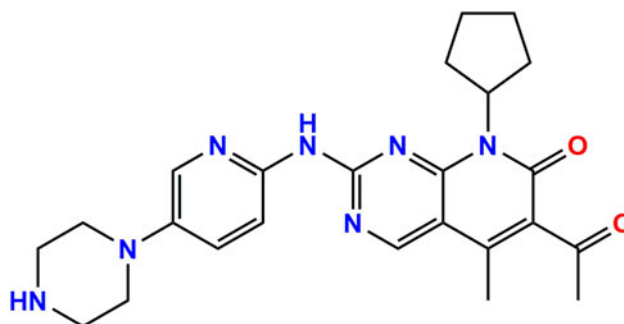


Figure 1. The molecular structure of palbociclib.

<sup>†</sup>Deceased

<sup>a)</sup>Author to whom correspondence should be addressed. Electronic mail: [ann.vologzhanina@gmail.com](mailto:ann.vologzhanina@gmail.com)

TABLE I. Crystal data and structure refinement for palbociclib.

Empirical formula	C <sub>24</sub> H <sub>29</sub> N <sub>7</sub> O <sub>2</sub>
Formula weight	447.52
Temperature (K)	295
Crystal system	Monoclinic
Space group	<i>P2<sub>1</sub>/c</i>
a (Å)	11.3133(2)
b (Å)	5.62626(9)
c (Å)	35.9299(9)
$\alpha$ (°)	90
$\beta$ (°)	101.5071(12)
$\gamma$ (°)	90
Volume (Å <sup>3</sup> )	2241.03(8)
Z	4
$\rho_{\text{calc}}$ (g cm <sup>-3</sup> )	1.327
<i>F</i> (000)	952
Radiation	Synchrotron ( $\lambda = 0.750271$ )
2 $\theta$ range for data collection (°)	2.00 to 30.0
Data/restraints/parameters	5601/90/141
Goodness-of-fit on <i>F</i> <sup>2</sup>	0.135
<i>R</i> -Bragg (%)	0.267
Final <i>R</i> indexes (%)	<i>R</i> <sub>wp</sub> = 0.758 <i>R</i> ' <sub>wp</sub> = 0.560 <i>R</i> <sub>p</sub> = 0.565 <i>R</i> ' <sub>p</sub> = 0.931
Residual density (e Å <sup>-3</sup> )	-0.10(3), 0.11(3)

'Bruker TOPAS 5 User Manual', 2014). The systematic absences suggested the space group *P2<sub>1</sub>/c*, which was confirmed by successful solution and refinement of the structure. A molecular model of palbociclib was taken from bis(palbociclib) oxalate dihydrate crystal structure (Katiyar et al., 2021) and converted into a Fenske–Hall Z-matrix file using OpenBabel (O'Boyle et al., 2011). A simulated annealing algorithm of Topas 5.0 was applied to find the positions of non-hydrogen atoms of palbociclib in an asymmetric unit. The solution result was used as a starting geometry for the periodic density functional theory (DFT) calculations at the Perdew–Baron–Erzenhopf (PBE) exchange–correlation functional level with a fixed unit cell using VASP 5.4.1 (Kresse and Hafner, 1993, 1994; Kresse and Furthmüller, 1996a, 1996b). Atomic cores were described using PAW potentials

(Blöchl, 1994; Joubert, 1999). Valence electrons were described in terms of a plane-wave basis set.

Optimization result with the fixed unit cell was used as the starting geometry and the sources of bond and angle restraints in the Rietveld refinement (Rietveld, 1967) for synchrotron powder XRD data. Atomic coordinates were taken from the PBE-PAW optimized model and refined with the Topas 5.0 software. Isotropic displacement parameters were constrained to be equal for all carbon atoms, all oxygen, and all nitrogen atoms. The positions of the hydrogen atoms were calculated geometrically and refined in the riding model with  $U_{\text{iso}}(\text{H}) = 1.2U_{\text{iso}}(\text{X})$ . The final *R*-values are listed in Table I along with the corresponding values of Rietveld refinement results. The Rietveld plot is given in Figure 2.

### A. Computational methods

The plane wave calculations were carried out in the VASP 5.4.1 program package (Kresse and Hafner, 1993, 1994; Kresse and Furthmüller, 1996a, 1996b). The PBE method (Perdew et al., 1999) and projected augmented waves (PAW) (Kresse and Joubert, 1999; Kresse and Hafner, 2000) were used. Valence electrons (2*s* and 2*p* for O, N, and C atoms; 1*s* for H) were described in terms of a plane-wave basis set. The kinetic energy cutoff for the wave functions was set to 800 eV. Automatic *k*-point sampling was used. The total energy and force convergence thresholds were set to 10<sup>-6</sup> and 10<sup>-4</sup> eV, respectively. The crystal structures from the powder X-ray diffraction experiment were used as the starting geometry for the calculations. The geometry optimizations were carried out with the lattice parameters fixed at their refined crystallographic values. The output files with the relaxed geometries were converted to a res-file using VESTA (Momma and Izumi, 2011).

### III. RESULTS AND DISCUSSION

The asymmetric unit of palbociclib contains one molecule (Figure 3). The root-mean-square Cartesian displacement of the non-H atoms in the Rietveld-refined model and VASP-optimized structures is 0.070 Å (Figure 4); the maximum

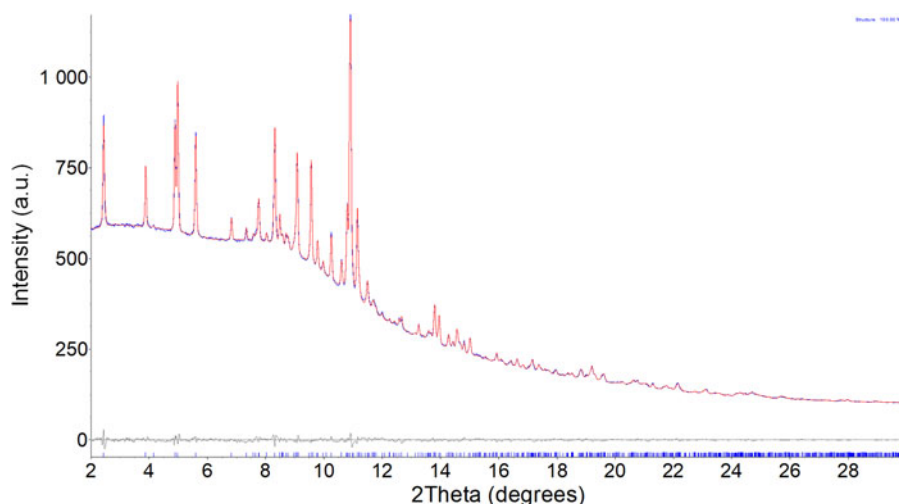


Figure 2. The Rietveld plot for the refinement of palbociclib. The blue and red lines represent the observed data points and the calculated pattern, respectively. The difference curve is gray.

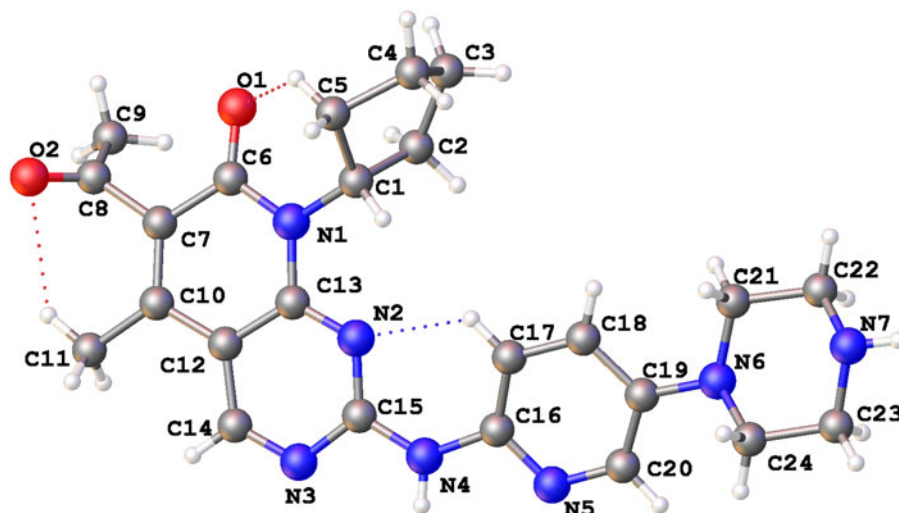


Figure 3. Asymmetric unit of palbociclib, with the atom numbering.

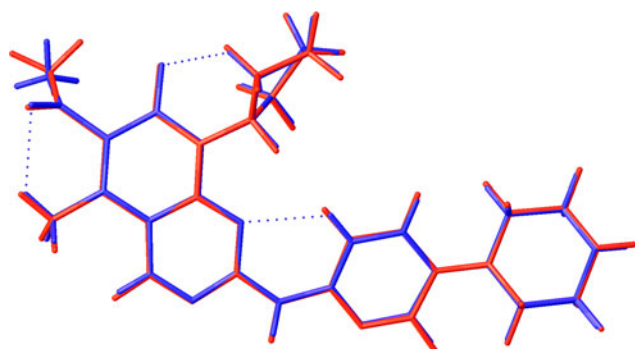


Figure 4. Comparison of the Rietveld-refined (red) and VASP-optimized (blue) structures of palbociclib.

deviation of non-H atoms are 0.133 and 0.153 Å at O2 and C9 atoms of the acetyl group. Besides, positions of hydrogen atoms of methyl groups also differ. The atomic displacement is within the typical range for correct structures (van de Streek and Neumann, 2014). Almost all of the bond distances and bond angles in the experimental model fall within the normal ranges indicated by a Mercury/Mogul Geometry check (Macrae et al., 2020). The C6–N1, C15–N3, and C12–C13 distances of 1.422, 1.379, and 1.432 Å are flagged as unusual; however, these correspond well with the distances from the VASP model (1.429, 1.375, and 1.426 Å).

Piperazinyl realizes the chair conformation (Figure 3). The plane-to-plane twist angle between the pyridine and pyrido[2,3-d]pyrimidine is 16.7(1)°. The cyclopentyl ring is in the twist conformation with C4 and C5 shift from the C1–C2–C3 mean plane of 0.241(6) and –0.463(6) Å. Palbociclib conformations in free base and previously reported single-crystal salts and cocrystals are visualized in Figure 5. The pyridine and pyridopyrimidine heterocycles are nearly coplanar, while the positions of acetyl, cyclopentyl, and piperazinyl groups strongly differ in different solids. Nevertheless, the piperazinyl ring is always in the chair conformation, and the cyclopentyl ring demonstrates lability both through different conformations, and prominent thermal motion.

Each molecule takes part in strong N–H...N-bonding. Parameters of these bonds for the theoretical model are listed



Figure 5. Palbociclib conformations in free base palbociclib (red), kaempferol palbociclib (orange, Zhou et al., 2023), bis(palbociclib) oxalate dihydrate (green, Katiyar et al., 2021), palbociclib methanesulfonate monohydrate (blue, Allu et al., 2024), palbociclib benzenesulfonate hemihydrate (purple, Allu et al., 2024), and palbociclib ethanesulfonate (magenta, Allu et al., 2024) structures. H atoms are omitted for clarity.

in Table II. Neighboring molecules of palbociclib are connected to dimers through an inversion center by means of two N4–H4...N2 bonds supported by two C5–H5...N5 interactions. The dimers are further connected by N7–H7a...N7 hydrogen bonds into infinite layers parallel with (001) planes (Figure 6). Besides, the molecules are involved in weak C–H...O bonding which connects the layers into a 3D framework.

Patent US10329290B2 publishes the characteristic peaks for palbociclib free base crystal form A at  $2\theta$  angles of  $8.0^\circ \pm 0.2^\circ$ ,  $10.1^\circ \pm 0.2^\circ$ ,  $10.3^\circ \pm 0.2^\circ$ ,  $11.5^\circ \pm 0.2^\circ$  (for Cu  $K\alpha$  radiation). The crystal form B has the characteristic peaks at  $2\theta$  angles of  $6.0^\circ \pm 0.2^\circ$ ,  $10.9^\circ \pm 0.2^\circ$ ,  $12.8^\circ \pm 0.2^\circ$ ,  $16.4^\circ \pm 0.2^\circ$ , and  $19.8^\circ \pm 0.2^\circ$  for Cu  $K\alpha$  radiation. The calculated pattern for

TABLE II. Hydrogen bonds (VASP 5.4.1) of palbociclib.

D–H...A	D–H (Å)	H...A (Å)	D...A (Å)	$\angle(\text{DHA})$ (°)
N4–H4...N3	1.046	1.921	2.967	179.8
N7–H7b...N7	1.036	2.266	3.294	170.9
C14–H14...N5	1.094	2.433	3.341	139.5
C5–H5a...O1	1.094	2.253	2.943	118.9
C11–H11c...O2	1.092	2.325	3.101	126.5



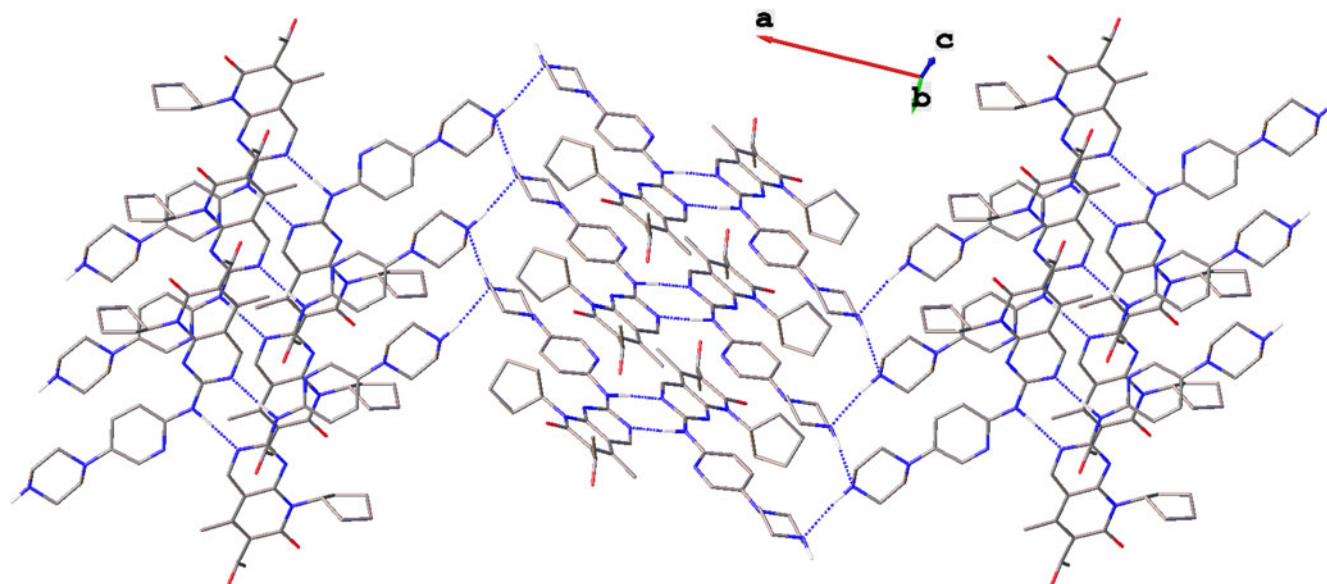


Figure 6. Fragment of N–H...N bonded layers in palbociclib. H-bonds are depicted with dotted lines.

our model for Cu  $K\alpha$  radiation comprises the characteristic peaks at  $2\theta = 5.02^\circ$ ,  $7.98^\circ$ ,  $10.02^\circ$ ,  $10.24^\circ$ ,  $11.52^\circ$ , etc. (Supplementary Figure S1) which correspond to the anhydrous form A of palbociclib.

The volume per palbociclib molecule is equal to its molecular Voronoi polyhedron  $V_{VP} = 554.7 \text{ \AA}^3$ . The molecular Voronoi polyhedron is expected to be constant for a molecule in a different environment (Baburin and Blatov, 2004; Prokaeva et al., 2009). Indeed, for palbociclib molecule in a cocrystal with kaempferol  $V_{VP}$  obtained using ToposPro package (Blatov et al., 2014) is equal to  $560.3 \text{ \AA}^3$  (Zhou et al., 2023). The  $V_{VP}$  value of palbociclib cations in bis(palbociclib) oxalate dihydrate ( $565.0 \text{ \AA}^3$  (Katiyar et al., 2021)) and palbociclib ethanesulfonate ( $567.9 \text{ \AA}^3$  (Allu et al., 2024)) is also close to the value of free base palbociclib, while in palbociclib methanesulfonate monohydrate ( $580.2 \text{ \AA}^3$  (Allu et al., 2024)) and palbociclib benzenesulfonate hemihydrate ( $590.1 \text{ \AA}^3$  (Allu et al., 2024)), it is higher.

#### IV. DEPOSITED DATA

The powder pattern of the title compound from this synchrotron data set has been submitted to ICDD for inclusion in the Powder Diffraction File. The CIF files containing the results of the Rietveld refinement (including the raw data) and the DFT geometry optimization were deposited with the ICDD and the CSD (CCDC 2363921) The data can be requested at [pdj@icdd.com](mailto:pdj@icdd.com) and [www.ccdc.cam.ac.uk/structures](http://www.ccdc.cam.ac.uk/structures), respectively.

#### SUPPLEMENTARY MATERIAL

The supplementary material for this article can be found at <https://doi.org/10.1017/S0885715624000411>.

#### ACKNOWLEDGEMENTS

This research was funded by the Russian Science Foundation, Grant No. 23-73-00027.

#### CONFLICTS OF INTEREST

The authors declare no conflicts of interest.

#### REFERENCES

- Allu, S., J.-H. An, B. J. Park, and W.-S. Kim. 2024. "Improving Dissolution Rate and Solubility of Palbociclib Salts/Cocrystal for Anticancer Efficacy." *Journal of Molecular Structure* 1305 (6): 137756. doi:10.1016/j.molstruc.2024.137756.
- Baburin, I. A., and V. A. Blatov. 2004. "Sizes of Molecules in Organic Crystals: The Voronoi–Dirichlet Approach." *Acta Crystallographica Section B: Structural Science* 60 (4): 447–52. doi:10.1107/S0108768104012698.
- Blatov, V. A., A. P. Shevchenko, and D. M. Proserpio. 2014. "Applied Topological Analysis of Crystal Structures with the Program Package ToposPro." *Crystal Growth & Design* 14 (7): 3576–86. doi:10.1021/cg500498k.
- Blöchl, P. E. 1994. "Projector Augmented-Wave Method." *Physical Review B* 50 (24): 17953–79. doi:10.1103/PhysRevB.50.17953.
- "Bruker TOPAS 5 User Manual". 2014. Karlsruhe, Germany: Bruker AXS GmbH.
- Buikin, P. A., A. V. Vologzhanina, R. A. Novikov, and A. A. Korlyukov. 2024a. "9-Ethyl-6,6-Dimethyl-8-[4-(Morpholin-4-Yl)Piperidin-1-Yl]-11-Oxo-6,11-Dihydro-5H-Benzo[b]Carbazole-3-Carbonitrile Hydrochloride." *Molbank* 2024 (1): M1759. doi:10.3390/M1759.
- Buikin, P., A. Korlyukov, E. Kulikova, R. Novikov, and A. Vologzhanina. 2024b. "Crystal Structure of Rilpivirine Hydrochloride,  $N_6H_{19}C_{22}Cl$ ." *Powder Diffraction* 39 (3): 151–8. doi:10.1017/S0885715624000228.
- Coelho, A. A. 2003. "Indexing of Powder Diffraction Patterns by Iterative Use of Singular Value Decomposition." *Journal of Applied Crystallography* 36 (1): 86–95. doi:10.1107/S0021889802019878.
- Fan, H., X. Guo, L. Huang, and H. Gu. 2019. "Preparation Methods for Palbociclib Free Base Crystal Form A and Crystal Form B." United States Patent US10329290B2. <https://patents.google.com/patent/US10329290B2/en?q=US10329290B2>.
- Fan, H., X. Guo, L. Huang, and H. Gu. 2020. "Preparation Methods for Palbociclib Free Base Crystal Form A and Crystal Form B." United States Patent US10766895B2. <https://patents.google.com/patent/US10766895B2/en?q=US10766895B2>.
- Finn, R. S., H. Dering, D. Conklin, O. Kalous, D. J. Cohen, A. J. Desai, C. Ginther, M. Atefi, I. Chen, C. Fowst, G. Los, and D. J. Slamon. 2009. "PD 0332991, a Selective Cyclin D Kinase 4/6 Inhibitor, Preferentially Inhibits Proliferation of Luminal Estrogen Receptor-Positive Human Breast Cancer Cell Lines in Vitro." *Breast Cancer Research* 11 (5): R77. doi:10.1186/bcr2419.

- Goloveshkin, A. S., A. A. Korlyukov, and A. V. Vologzhanina. 2021. "Novel Polymorph of Favipiravir — An Antiviral Medication." *Pharmaceutics* 13 (2): 139. doi:10.3390/pharmaceutics13020139.
- Goloveshkin, A. S., E. S. Kulikova, R. A. Novikov, A. V. Vologzhanina, and A. A. Korlyukov. 2024. "Crystal Structure of Nilotinib Hydrochloride Monohydrate According to Powder X-Ray Diffraction Data." *Journal of Structural Chemistry* 65 (3): 585–95. doi:10.1134/S0022476624030132.
- Ibrahim, F. M. L., M. P. Mullarney, R. M. Shanker, B. R. Spong, and J. Wang. 2016. "Solid Dosage Forms of Palbociclib." World Intellectual Property Organization Patent WO2016193860A1. <https://patents.google.com/patent/WO2016193860A1/en?q=WO2016193860A1>
- Joubert, D. 1999. "From Ultrasoft Pseudopotentials to the Projector Augmented-Wave Method." *Physical Review B - Condensed Matter and Materials Physics* 59 (3): 1758–75. doi:10.1103/PhysRevB.59.1758.
- Katiyar, D., S. Ahamad, S. G. Dash, S. Tripathi, A. Arora, and T. S. Thakur. 2021. "Understanding the Guest Binding in the Cucurbit[7]Uril Inclusion Complexes of CDK4/6 Inhibitors, Palbociclib, and Ribociclib from a Combined Experimental and Computational Study." *Journal of Molecular Structure* 1241 (10): 130637. doi:10.1016/j.molstruc.2021.130637.
- Kresse, G., and J. Furthmüller. 1996a. "Efficiency of Ab-Initio Total Energy Calculations for Metals and Semiconductors Using a Plane-Wave Basis Set." *Computational Materials Science* 6 (1): 15–50. doi:10.1016/0927-0256(96)00008-0.
- Kresse, G., and J. Furthmüller. 1996b. "Efficient Iterative Schemes for Ab Initio Total-Energy Calculations Using a Plane-Wave Basis Set." *Physical Review B - Condensed Matter and Materials Physics* 54 (16): 11169–86. doi:10.1103/PhysRevB.54.11169.
- Kresse, G., and J. Hafner. 1993. "Ab Initio Molecular Dynamics for Liquid Metals." *Physical Review B* 47 (1): 558–61. doi:10.1103/PhysRevB.47.558.
- Kresse, G., and J. Hafner. 1994. "Ab Initio Molecular-Dynamics Simulation of the Liquid-Metal–Amorphous-Semiconductor Transition in Germanium." *Physical Review B* 49 (20): 14251–69. doi:10.1103/PhysRevB.49.14251.
- Kresse, G., and J. Hafner. 2000. "First-Principles Study of the Adsorption of Atomic H on Ni (111), (100) and (110)." *Surface Science* 459 (3): 287–302. doi:10.1016/S0039-6028(00)00457-X.
- Kresse, G., and D. Joubert. 1999. "From Ultrasoft Pseudopotentials to the Projector Augmented-Wave Method." *Physical Review B* 59 (3): 1758–75. doi:10.1103/PhysRevB.59.1758.
- Macrae, C. F., I. Sovago, S. J. Cottrell, P. T. A. Galek, P. McCabe, E. Pidcock, M. Platings, G. P. Shields, J. S. Stevens, M. Towler, and P. A. Wood. 2020. "Mercury 4.0: From Visualization to Analysis, Design and Prediction." *Journal of Applied Crystallography* 53 (1): 226–35. doi:10.1107/S1600576719014092.
- Momma, K., and F. Izumi. 2011. "VESTA 3 for Three-Dimensional Visualization of Crystal, Volumetric and Morphology Data." *Journal of Applied Crystallography* 44 (6): 1272–76. doi:10.1107/S0021889811038970.
- Morris, M. C., H. F. McMurdie, E. H. Evans, B. Paretzkin, H. S. Parker, H. S. Pyrras, and C. R. Hubbard. 1984. "Standard X-Ray Diffraction Powder Patterns: Section 20 - Data for 71 Substances." Gaithersburg, MD: National Institute of Standards and Technology. doi:10.6028/NBS.MONO.25-20.
- O'Boyle, N. M., M. Banck, C. A. James, C. Morley, T. Vandermeersch, and G. R. Hutchison. 2011. "Open Babel: An Open Chemical Toolbox." *Journal of Cheminformatics* 3 (1): 33. doi:10.1186/1758-2946-3-33.
- Perdew, J. P., S. Kurth, A. Zupan, and P. Blaha. 1999. "Accurate Density Functional with Correct Formal Properties: A Step Beyond the Generalized Gradient Approximation." *Physical Review Letters* 82 (12): 2544–47. doi:10.1103/PhysRevLett.82.2544.
- Prokaeva, M. A., I. A. Baburin, and V. N. Serezhkin. 2009. "On Methods to Determine the Surface Areas of Molecules." *Journal of Structural Chemistry* 50 (5): 867–72. doi:10.1007/s10947-009-0129-5.
- Rietveld, H. M. 1967. "Line Profiles of Neutron Powder-Diffraction Peaks for Structure Refinement." *Acta Crystallographica* 22 (1): 151–52. doi:10.1107/S0365110X67000234.
- Rocca, A., A. Farolfi, S. Bravaccini, A. Schirone, and D. Amadori. 2014. "Palbociclib (PD 0332991): Targeting the Cell Cycle Machinery in Breast Cancer." *Expert Opinion on Pharmacotherapy* 15 (3): 407–20. doi:10.1517/14656566.2014.870555.
- Svetogorov, R. D. 2018. *Dionis – Diffraction Open Integration Software*. Moscow: National Research Center, Kurchatov Institute.
- Svetogorov, R. D., P. V. Dorovatovskii, and V. A. Lazarenko. 2020. "Belok/ XSA Diffraction Beamline for Studying Crystalline Samples at Kurchatov Synchrotron Radiation Source." *Crystal Research and Technology* 55 (5): 1900184. doi:10.1002/crat.201900184.
- van de Streek, J., and M. A. Neumann. 2014. "Validation of Molecular Crystal Structures from Powder Diffraction Data with Dispersion-Corrected Density Functional Theory (DFT-D)." *Acta Crystallographica Section B: Structural Science, Crystal Engineering and Materials* 70 (6): 1020–32. doi:10.1107/S2052520614022902.
- Zhou, H., C. Duan, H. Qin, C. Huang, J. Hou, Y. Chen, J. Zhu, C. Xu, J. Jin, and T. Zhuang. 2023. "Synthesis and Structural Characterization of a Novel Palbociclib-Kaempferol Cocrystal with Improved Tabletability and Synergistic Antitumor Activity." *Journal of Molecular Structure* 1281 (6): 135101. doi:10.1016/j.molstruc.2023.135101.